Volume 1 | Number 1 | Jan 2013 | Pages 1–100

Journal of
Materials Chemistry A

Materials for energy and sustainability
www.rsc.org/materialsA

Li⁺
e⁻
e⁻
Li⁺
Li⁺
Li⁺

ROYAL SOCIETY
OF CHEMISTRY

ROYAL SOCIETY
OF CHEMISTRY

www.rsc.org/materialsA

ARTICLE TYPE

In situ growth of ultrafine tin oxide nanocrystals embedded in graphitized carbon nanosheets for high-performance lithium-ion batteries

Wei Fu, Fei-Hu Du, Kai-Xue Wang,* Tian-Nan Ye, Xiao Wei,* and Jie-Sheng Chen

Crystal-facet-induced formation method has been developed for the fabrication of graphitized carbon nanosheets (CNS) embedded with *in situ* generated ultrafine SnO_2 nanocrystals upon calcination in N_2 atmosphere. The obtained SnO_2/CNS composite exhibits superior electrochemical performance when used as anode material for lithium ion batteries. Cycled at high current densities of 0.5, 1.0 and 10.0 A g^{-1} for 50 cycles, the composite material delivers large discharge capacities of 826, 728, and 400 mAh g^{-1}, respectively. The graphitized carbon nanosheets could facilitate both ion and electron diffusion and act as an efficient buffer to accommodate the volume changes generated upon Li-ion insertion/extraction. The ultrafine SnO_2 nanocrystals can significantly shorten the diffusion distance of lithium ions and also provide a large contact area for the interface reaction between anode material and lithium-ion during lithiation or delithiation, leading to remarkably high specific capacity and good cycling stability.

Introduction

Lithium ion batteries (LIBs), which have been successfully used in portable electronic devices, have attracted considerable attention in the scientific and industrial fields due to its outstanding energy density and long cycle life. [1-6] To meet the increasing demand for high-performance batteries, much research attempt has been made to explore new electrode materials with novel nanostructures, particularly the nanocrystal-based materials. A key attractive feature of nanocrystal-based electrode materials is the small crystal size, which can significantly shorten the diffusion distance of lithium ions within the electrode and thus lead to enhanced rate capability. [7-10] Furthermore, huge volume variation with the insertion/extraction of lithium ions is the primary cause of degradation of anode materials upon cycling. [11-15] Taking advantage of the small particle size, nanocrystals can also effectively tolerate the degradation of anode materials caused by such volume expansion/contraction, ensuring improved cycling stability. [16-18]

However, ultrafine nanocrystals cannot be directly used as electrode material. The large electrodes/electrolyte contact interface raises the risk of secondary reactions involving the electrolyte decomposition and the formation of a thick gel-like polymeric layer, leading to the fast capacity fading and inferior rate capability. These issues are expected to be circumvented by immobilization of the nanocrystals into graphitized carbon nanosheets. The carbon nanosheets can lock the nanocrystals in their position, and buffer the volume variation upon cycling. The good dispersion of the nanocrystals within the carbon nanosheets can avoid the direct contact of the nanocrystals with the electrolyte, preventing the adverse reactions. Furthermore, the two-dimensional (2D) graphitized carbon nanosheets can facilitate the transport of electrons and lithium ions to the surfaces of nanocrystals, resulting in good conductivity and fast charge/discharge rate.

SnO_2 materials are regarded as promising anode candidates for high performance lithium-ion batteries considering their low charge-discharge potentials and high theoretical capacities. [19-21] Its specific capacity is about 780 mA h g^{-1}, more than twice as that of graphite. [22-24] However, the large volume change of approximately 250 % between the fully alloyed and dealloyed states leads to the pulverization and severe destruction of the electrode, resulting in fast fading of the capacity. [25,26] Herein, we describe the direct immobilization of SnO_2 ultrafine nanocrystals into graphitized carbon nanosheets through a simple crystal-facet-induced formation method. Graphitized carbon nanosheets embedded with *in situ* formed SnO_2 ultrafine nanocrystals are fabricated by simply heating the coating of tin tetrachloride/tin oleate complex on the surface of sodium sulphate crystals in N_2 atmosphere. Electrochemical evaluation reveals the excellent electrochemical performance of the SnO_2/CNS composite, including ultrafast transfer of lithium-ions and electrons, and the outstanding structure stability upon cycling.

Experimental section

Preparation of SnO_2/CNS composite

In a typical procedure, 0.72 g of tin tetachloride ($SnCl_4$, Acros) was dissolved in 2.0 mL of de-ionized water and then mixed with 1.22 g sodium oleate (TCI, 95%).The mixture was aged at 358 K for 3 h, leading to the formation of tin oleate. Then, 10.0 g of sodium sulphate (Aldrich, 98%) was added to the above mixture.
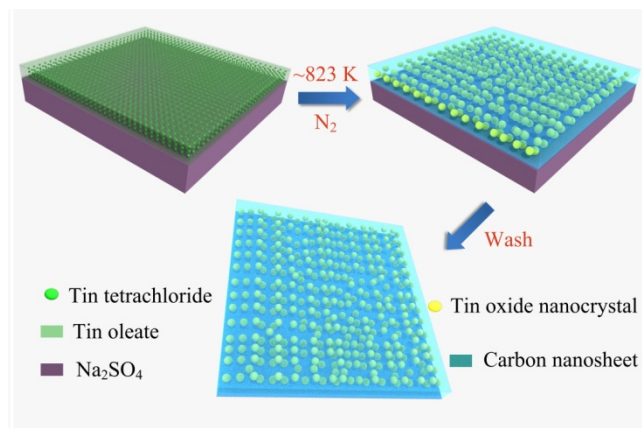
Scheme 1. Schematic representation of the preparation procedure of the SnO₂/CNS composite.

Upon gentle grounding, the mixture containing tin oleate was uniformly coated on the surface of sodium sulphate particles. The ground mixture was heated at 823 K with a ramping rate of 10 K min⁻¹ under a N₂ atmosphere for 1.0 h. After cooled down naturally, the product was washed with de-ionized water to remove sodium sulphate and then dried at 353 K for 12 h.

Characterization

The X ray diffraction (XRD) patterns were recorded on a D/max 2550VL/PC X-ray diffractometer (Rigaku, Japan) equipped with Cu Kα radiation (λ = 1.5406 Å, 40 kV, 30 mA). The Raman spectra were acquired using an inVia-reflex micro-Raman spectrometer (Renishaw, UK) with a 532 nm wavelength incident laser. X-ray photoelectron spectroscopy (XPS) was performed on an AXIS Ultra DLD spectrometer (Kratos, Japan) with Al Kα radiation (hν = 1486.6 eV). The thermogravimetric analysis (TGA) was carried out on a Perkin Elmer TGA 7 thermogravimetric analyzer. The morphology and crystal lattice of samples were characterized by transmission electron microscopy (TEM, JEOL, JEM-2100, with an accelerating voltage of 100 kV), high-resolution transmission electron microscopy (HRTEM, JEOL, JEM-2100, with an accelerating voltage of 200 kV), respectively. The scanning electron microscopic (SEM) images were obtained with a FEI Nova NanoSEM 2300.

Electrochemical measurements

The working electrode was fabricated as following. First, the as-obtained sample (70 wt %), Super-P carbon black (15 wt %, Timcal), and sodium carboxymethyl cellulose (15 wt %) were mixed in an ethanol/water solution to form a slurry. The slurry was spread onto a Cu foil by a doctor blade method, followed by drying in vacuum at 343 K for 8 h. A lithium foil acted as both the counter and reference electrodes, and a microporous polypropylene membrane (Celgard 2500) was used as the separator. CR2016 coin cells were assembled in an argon-filled glove box with both moisture and oxygen contents below 1.0 ppm. The electrolyte was 1.0 M LiPF₆ in the mixture of ethylene carbonate (EC) and dimethyl carbonate (DMC) (1:1 in volume ratio). The galvanostatic charge and discharge experiment was performed with a battery tester LAND-CT2001A in the voltage range of 0.01 ~ 3.0 V at room temperature. The cyclic voltammetry was conducted on a CHI660B electrochemical workstation at a scanning rate of 0.5 mV/s in a potential range of 0.01 ~ 3.0 V (vs. Li/Li⁺).

Results and Discussion

The typical synthetic procedure is depicted in Scheme 1. First, a mixture containing tin oleate and tin tetrachloride was obtained by aging SnCl₄ and sodium oleate with the presence of a small amount of de-ionized water at 358 K for 3 h. The formed mixture was then uniformly coated onto the surface of sodium sulphate crystals. The facets of the sodium sulphate crystals function as a 2D template to induce the formation of the SnO₂/CNS composite. Upon calcination in a tube furnace in N₂ atmosphere, carbon nanosheets and SnO₂ nanocrystals formed through the carbonization of the oleate complex and the transformation of tin species on the surface of sodium sulphate particles, respectively. After removal of Na₂SO₄ substrate by simply washing with de-ionized water, the SnO₂/CNS composite with ultrafine SnO₂ nanocrystals embedded in graphitized carbon nanosheets was obtained.
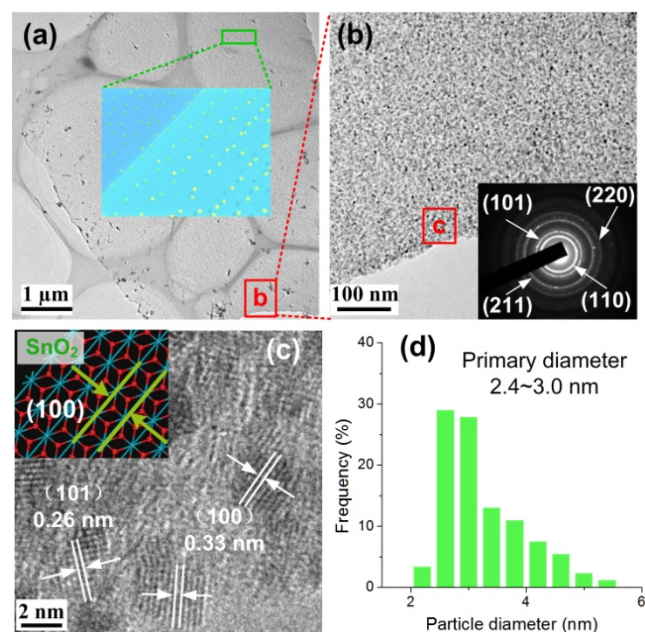
Fig. 1 (a and b) TEM images of SnO₂/CNS composite. Inset of a: diagrammatic sketch of inner structure. Inset of b: corresponding SAED pattern. (c) High-resolution TEM image and (d) Particle size distribution.

The morphology and textural details of the as-prepared hybrid are observed by TEM. The SnO₂/CNS composite sample is uniform films with large area (Fig. 1a), indicating the templating effect of the facets of the sodium sulphate crystals. The magnified TEM image shows that ultrafine tin oxide nanocrystals are uniformly dispersed within the carbon nanosheets (Fig. 1b). The corresponding selected area electron diffraction (SAED) pattern presents a series of diffraction rings which can be indexed to the (110), (101), (211) and (220) planes, respectively of tetragonal-

structured SnO_2 (Inset of Fig. 1b).[27,28] The presence of the diffraction rings in the SAED pattern suggests the polycrystalline nature of SnO_2. The HRTEM image of the sample is shown in Fig. 1c. The lattice fringes with spacings of 0.33 nm and 0.26 nm can be clearly observed, corresponding to the (110) and (101) planes of tetragonal-structured SnO_2, respectively, consistent with the SAED analysis. The schematic representation of (110) crystal plane of SnO_2 is depicted in the inset of Fig. 1c. The particle size distribution of SnO_2 is measured based on the HRTEM image shown in Fig. S1 (Fig. 1d). The particle size is mainly within the range of 2.4 ~ 3.0 nm in diameter, indicting the SnO_2 nanocrystals *in situ* generated are ultrafine and the particle size distribution is quite uniform.

The SEM image shows that SnO_2/CNS composite is rather uniform and large (Fig. 2a). The high-resolution SEM image in Fig. 2b shows that the ultrafine SnO_2 nanocrystals are immobilized and well dispersed in the matix of carbon nanosheets. It is assumed that the carbon nanosheets may lock the nanocrystals in their position and prevent the aggregation and further crystal growth of the nanocrystals during the calcination process. The good dispersion of the nanocrystals within the carbon nanosheets can avoid the direct contact of the nanocrystals with the electrolyte, preventing the adverse reactions.
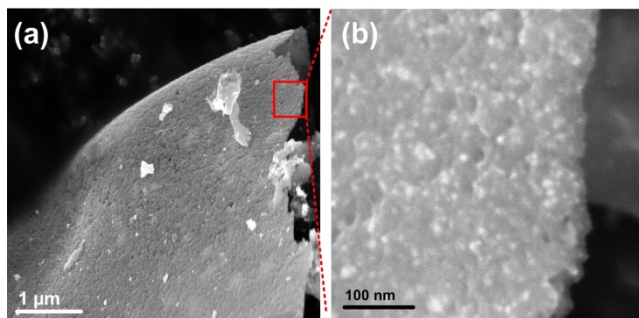
Fig. 2 (a and b) SEM images of tin oxide nanocrystals embedded in carbon nanosheet.

The XRD pattern of the hybrid is shown in Fig.3a. The well resolved diffraction peaks located at 26.83°, 33.9° and 51.8° can be readily indexed to the (110), (101) and (211) diffractions diffractions, respectively of the tetragonal-structured SnO_2 with a space group of P42/mnm, in good agreement with that of SnO_2 (JCPDS card No. 41-1445). The Raman spectrum of the sample is shown in Fig. 2b. Two distinguishable peaks at around 1589 and 1335 cm^{-1} are ascribed to the vibration of sp^2 carbon atoms in a 2D hexagonal lattice (the G-band) and to defects and disorder in the hexagonal graphitic layers (the D-band).[29] The low intensity ratio I_D/I_G indicates that the obtained carbon nanosheets are composed of nanocrystalline graphite. As determined by the TGA analysis, the content of CNS in the SnO_2/CNS composite is approximately 29 wt%.

The XPS technique was used to investigate the nature of carbon in the SnO_2/CNS composite. The XPS survey spectrum in Fig. 3c represents that the sample is only composed of Sn, C and O elements, indicating the complete removal of sodium sulphate after simply washing with de-ionized water. The high-resolution XPS spectrum of C 1s is depicted in Fig. 3d. It can be

deconvoluted into four components. The main peak at 284.5 eV is attributed to sp^2-hybridized graphene, while the weak peak at 284.8 eV is assigned to sp^3-hybridized carbon.[30] Two weak peaks at 286.1 and 288.5 eV are assigned to oxidized carbons. The high area ratio of two peaks at 284.5 and 284.8 reveals the high graphitization degree of carbon nanosheets in the SnO_2/CNS composite, in good agreement with the Raman analysis. The XPS spectrum of Sn 3d shows two peaks at 495.6 and 487.3 eV, attributed to Sn $3d_{5/2}$ and $3d_{3/2}$, respectively (Fig. S2). These binding energies are all consistent with the reported values for the SnO_2 crystal.[31]
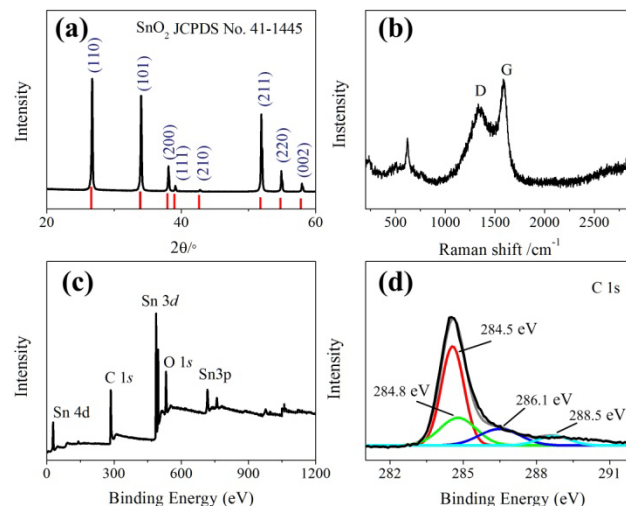
Fig. 3 (a) XRD pattern and (b) Raman spectra. (c, d) XPS survey spectrum and XPS C1s spectrum of the SnO_2/CNS composite.

Intrigued by the structural features, the lithium storage properties of the SnO_2/CNS composite as a potential anode material have been evaluated. The initial three consecutive cyclic voltammograms (CVs) of the hybrids are shown in Fig. 4a. In the first cathodic scan, the weak peak at 1.15 V was due to the formation of the solid electrolyte interphase (SEI). The obvious peak is present around 0.51 V, which is attributed to the irreversible reaction: $SnO_2 + 4Li^+ + 4e^- \rightarrow Sn + 2Li_2O$. The broad band extending to 0 V corresponded to the formation of nonstoichiometric LixSn alloys ($Sn + xLi^+ + xe^- \rightarrow Li_xSn$, $0 \le x \le 4.4$). In the reverse anodic curve, a large oxidation peak at 0.72 V is attributed to the electrochemical reactions of Sn with Li to form Li-Sn alloys (Li_xSn). In the following cycles, the stable oxidation and reduction peaks are clearly observed. The CV curves with distinct redox peaks are consistent with those reported in the literature for SnO_2 materials.[32, 33] The stable redox peaks upon cycling indicated that the stability of the hybrid structure upon lithiation and delithiation.

Fig. 4b shows galvanostatic discharge/charge profiles of the SnO_2/CNS composite at a high current density of 0.5 A g^{-1} in the voltage range of 0.01 ~ 3.0 V (vs. Li^+/Li). The initial discharge and charge capacities of the hybrid are 1252 and 850 mA h g^{-1}, respectively, giving a coulombic efficiency of 68 %. The irreversible capacity of 32 % is due to the formation of Li_2O, an inorganic solid electrolyte interface (SEI) film and decomposition of electrolyte. The coulombic efficiency increases to over 96 % in

the subsequent cycles. Compared with the SnO_2-based electrode materials reported in the literature,[34-37] The SnO_2/CNS composite shows distinctly high coulombic efficiency and large capacities at high current densities, attributing to the unique structure of the composite.
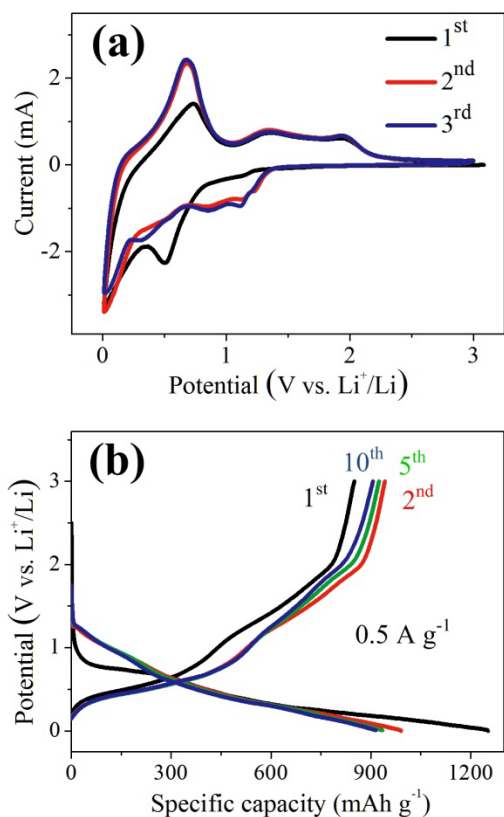
Fig. 4 Battery performance of SnO_2/CNS composite. (a) Cyclic voltammograms at a scanning rate of 0.5 mV s^{-1} over a voltage range of 0.01-3.0 V. (b) Galvanostatic charge-discharge profiles at 0.5 A g^{-1} between 0.01-3.0 V.

The cycling performance of the SnO_2/CNS composite is tested at high current densities of 0.5, 1.0 and 10.0 A g^{-1}. The variation of the specific discharge capacities is plotted as a function of the cycling number (Fig. 5a). Cycled at 0.5, 1.0 and 10.0 A g^{-1} for 50 cycles, large discharge capacities of approximately 826, 728, and 400 mAh g^{-1}, respectively, approximately 88 %, 84 %, and 72 % of the corresponding initial discharge capacity are still retained, indicating the excellent cycling stability of the SnO_2/CNS composite. To the best of our knowledge, such high energy capacity and stable cycling property at a high current density of 10.0 A g^{-1} have never been reported so far for Sn-based anode materials in the literature. The slight capacity decay over the first 3 cycles is attributed to the consumption of lithium-ion for the formation of Li_2O inactive phase and the SEI layer. The superb electrochemical performance is ascribed to the large area of the hybrid anode and the structure stability during cycling.

In addition to the remarkable cycleability, the SnO_2/CNS composite also exhibit excellent rate performance. Fig. 5b shows the variations of the reversible capacities with current densities and discharge-charge cycles. The cells were first cycled at 0.1 A

g^{-1} for 5 cycles, followed by cycling at current densities increasing stepwise to as high as 10 A g^{-1}. A reversible capacity of approximately 1083 mA h g^{-1} is achieved at a current density of 0.1 A g^{-1}, 918 mAh g^{-1} at 0.5 A g^{-1}, 722 mAh g^{-1} at 2.0 A g^{-1}, and 393 mAh g^{-1} at 10.0 A g^{-1}, respectively. Decreasing the current density back to 0.1 A g^{-1} after cycling at 10.0 A g^{-1}, reversible capacities of 1016 mA h g^{-1} is restored, indicating the good reversibility and structural stability of the SnO_2/CNS composite anode.
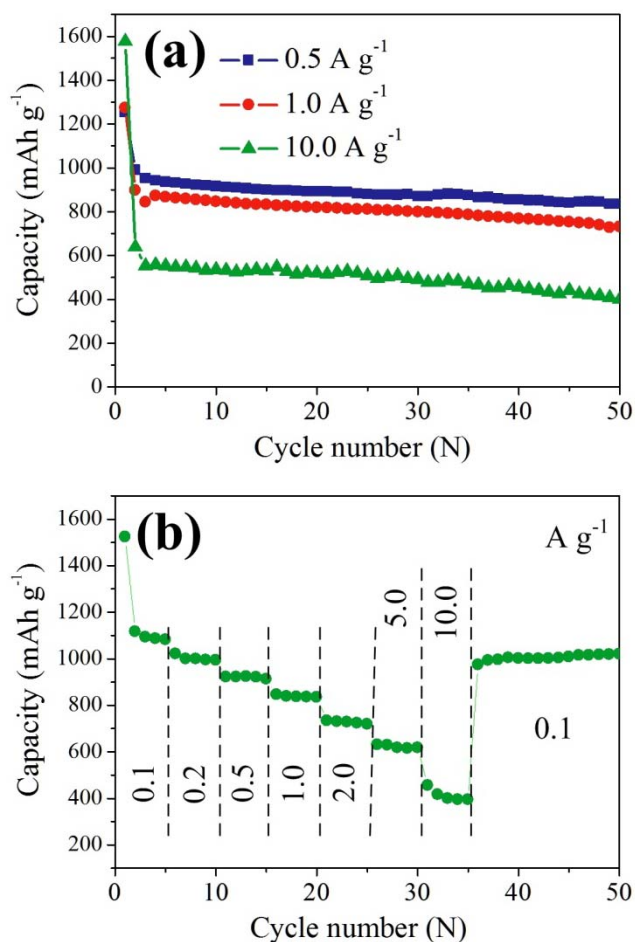
Fig. 5 (a) Cycling performance of the SnO_2/CNS composite at high current density of 0.5, 1.0 and 10.0 A g^{-1}. (d) Rate performance at various current densities of 0.1, 0.2, 0.5, 1.0, 2.0, 5.0 and 10.0 A g^{-1}.

Compared with other SnO_2-based electrode materials reported in the literature,[34-37] the SnO_2/CNS composite exhibits distinctly higher specific capacity, better cycleabiltiy and excellent rate performance, which are associated with the unique structural feature of the composite. The ultrafine SnO_2 nanocrystals significantly shorten the diffusion distance of lithium ions and also provide a large contact area for the interface reaction between anode material and lithium-ion during lithiation or delithiation, enhancing the rate capability of the composite. The graphitized carbon nanosheets which stabilize SnO_2 nanocrystals enhance the electrical conductivity of the composite, contributing

to the high rate performance. As shown in the schematic illustration in Fig. 6, ultrafine SnO_2 nanocrystals embedded in the graphitized carbon nanosheets can accommodate the huge volume variation of SnO_2 caused by the insertion and extraction of lithium ions and avoid the pulverization of the anode upon cycling, ensuring the good structure stability and cycleability. The carbon nanosheets can also prevent the direct contact of the ultrafine SnO_2 nanocrystals with the electrolyte and thus the decomposition of the electrolyte molecules on the high active surface of the nanoparticles, reducing the irreversible capability. As a result, excellent electrochemical performance is achieved for this SnO_2/CNS composite.
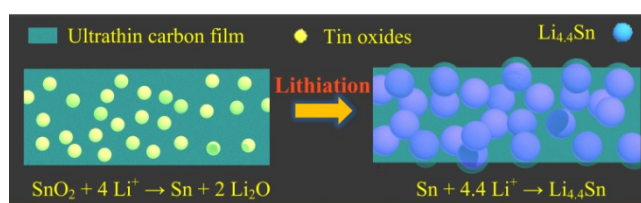
Fig. 6 Schematic representation of SnO_2/CNS composite before and after lithiation.

Conclusions

We have developed a simple crystal-facet-induced formation method to prepare a SnO_2/CNS composite. The calcination of the tin oleate coating on the crystal surface of sodium sulphate leads to the formation of graphitized carbon nanosheets embedded with ultrafine SnO_2 nanocrystals *in situ* generated. As demonstrated by the galvanostatic charge/discharge tests, the SnO_2/CNS composite exhibits large specific capacity, good cycling stability and excellent rate capabilit. Large discharge capacities of approximately 730 and 400 mA h g^{-1} are retained after 50 cycles at high current densities of 1.0 and 10.0 A g^{-1}, respectively. It is found that the ultrafine SnO_2 nanocrystals can significantly shorten the diffusion distance of lithium ions and also provide a large contact area for the interface reaction between anode material and lithium-ion during lithiation or delithiation. In addition to the enhanced electrical conductivity, the graphitized carbon nanosheet can also act as an efficient buffer to accommodate the volume changes generated upon Li-ion insertion/extraction. This work provides a simple but efficient route for the fabrication of novel anode materials for high-performance lithium-ion batteries.

Notes and references

School of Chemistry and Chemical Engineering, Shanghai Jiao Tong University, Shanghai, P. R. China. Fax: (+86)-21-54741297; Tel: (+86)-21-34201273; E-mail: k.wang@sjtu.edu.cn, weixiao@sjtu.edu.cn.
††Electronic Supplementary Information (ESI) available: The TEM image, the high-resolution Sn 3d XPS spectrum of the SnO_2/CNS composite are available. See DOI: 10.1039/b000000x/.

Acknowledgements

References

1. M. Armand and J. M. Tarascon, *Nature*, 2008, **451**, 652-657.
2. J. M. Tarascon and M. Armand, *Nature*, 2001, **414**, 359-367.
3. S. J. Ding, D. Y. Zhang, H. B. Wu, C. Z. Zhang and X. W. Lou, .*Nanoscale,* 2012, **4**, 3651-3654.
4. Y. Wang, Z. S. Feng, C. Zhang, L. Yu, J. J. Chen, J. Hu and X. Z. Liu, *Nanoscale*, 2013, **5**, 3704-3712.
5. Y. Wang, Z. S. Feng, J. J. Chen, C. Zhang, X. Jin and J. Hu, *Solid State Commun.*, 2012, **152**, 1577-1580.
6. M. S. Whittingham, *Chem. Rev.*, 2004, **104**, 4271-4301.
7. J. Yao, X. Shen, B. Wang, H. Liu and G. Wang, *Electrochem. Commun.,* 2009, **11**, 1849-1852.
8. Y. Li, B. Tan and Y. Wu, *Nano Lett.*, 2007, **8**, 265-270.
9. Z. S. Wu, W. Ren, L. Wen, L. Gao, J. Zhao, Z. Chen, G. Zhou, F. Li and H.-M. Cheng, *Nano*, 2010, **4**, 3187-3194.
10. F. H. Du, K. X. Wang, W. Fu, P. F. Gao, J. F. Wang and J. S. Chen, *J. Mater. Chem. A*, 2013, **1**, 13648-13654..
11. Y. M. Jiang, K. X. Wang, X. X. Guo, X. Wei, J. F. Wang and J. S. Chen, *J. Power Sources*, 2012, **214**, 298-302.
12. W. M. Zhang, J. S. Hu, Y. G. Guo, S. F. Zheng, L. S. Zhong, W. G. Song and L.-J. Wan, *Adv. Mater.*, 2008, **20**, 1160-1165.
13. N. Dimov, S. Kugino and M. Yoshio, *Electrochim. Acta*, 2003, **48**, 1579-1587.
14. R. Teki, M. K. Datta, R. Krishnan, T. C. Parker, T.-M. Lu, P. N. Kumta and N. Koratkar, *Small*, 2009, **5**, 2236-2242.
15. M. S. Park, S. A. Needham, G. X. Wang, Y. M. Kang, J. S. Park, S. X. Dou and H. K. Liu, *Chem. Mater.,* 2007, **19**, 2406-2410.
16. B. Wang, X. L. Wu, C. Y. Shu, Y. G. Guo and C. R. Wang, *J. Mater. Chem.,* 2010, **20**, 10661-10664.
17. Z. Wang, L. Zhou and X. W. Lou, *Adv. Mater.*, 2012, **24**, 1903-1911.
18. H. Li, L. Shi, Q. Wang, L. Chen and X. Huang, *Solid State Ionics*, 2002, **148**, 247-258.
19. M. S. Park, G. X. Wang, Y. M. Kang, D. Wexler, S. X. Dou and H. K. Liu, *Angew. Chem. Int. Ed.,* 2007, **119**, 764-767.
20. J. Liu, Y. Li, X. Huang, R. Ding, Y. Hu, J. Jiang and L. Liao, *J. Mater. Chem.,* 2009, **19**, 1859-1864.
21. J. S. Chen, Y. L. Cheah, Y. T. Chen, N. Jayaprakash, S. Madhavi, Y. H. Yang and X. W. Lou, *J. Phys. Chem. C*, 2009, **113**, 20504-20508.
22. H. X. Zhang, C. Feng, Y. C. Zhai, K. L. Jiang, Q. Q. Li and S. S. Fan, *Adv. Mater.,* 2009, **21**, 2299-2304.
23. J. Liu, W. Li and A. Manthiram, *Chem. Commun.,* 2010, **46**, 1437-1439.
24. J. S. Chen, L. A. Archer and X. Wen Lou, *J. Mater. Chem.,* 2011, **21**, 9912-9924.
25. R. Liang, H. Cao, D. Qian, J. Zhang and M. Qu, *J. Mater. Chem.,* 2011, **21**, 17654-17657.
26. D. Deng, M. G. Kim, J. Y. Lee and J. Cho, *Energ. Environ. Sci.,* 2009, **2**, 818-837.
27. X. W. Lou, Y. Wang, C. Yuan, J. Y. Lee and L. A. Archer, *Adv. Mater.,* 2006, **18**, 2325-2329.
28. L. S. Zhang, L. Y. Jiang, H. J. Yan, W. D. Wang, W. Wang, W. G. Song, Y. G. Guo and L. J. Wan, *J. Mater. Chem.,* 2010, **20**, 5462-5467.
29. M. A. Pimenta, G. Dresselhaus, M. S. Dresselhaus, L. G. Cançado, A. Jorio and R. Saito, *Phys. Chem. Chem. Phys.,* 2007, **9**, 1276-1291.
30. D. Deng and J. Y. Lee, *Chem. Mater.,* 2008, **20**, 1841-1846.
31. H. J. Ahn, H. C. Choi, K. W. Park, S. B. Kim and Y. E. Sung, *J. Phys. Chem. B*, 2004, **108**, 9815-9820.
32. X. Li, X. Meng, J. Liu, D. Geng, Y. Zhang, M. N. Banis, Y. Li, J. Yang, R. Li, X. Sun, M. Cai and M. W. Verbrugge, *Adv. Funct. Mater.,* 2012, **22**, 1647-1654.
33. L. Ji, Z. Tan, T. Kuykendall, E. J. An, Y. Fu, V. Battaglia and Y. Zhang, *Energ. Environ. Sci.,* 2011, **4**, 3611-3616.
34. J. Deng, C. Yan, L. Yang, S. Baunack, S. Oswald, H. Wendrock, Y. Mei and O. G. Schmidt, *Nano*, 2013, **7**, 6948-6954.
35. J. S. Chen and X. W. Lou, *Small*, 2013, **9**, 1877-1893.
36. M. S. Park, Y. M. Kang, G. X. Wang, S. X. Dou and H. K. Liu, *Adv. Funct. Mater.,* 2008, **18**, 455-461.
37. C. Wang, Y. Zhou, M. Ge, X. Xu, Z. Zhang and J. Z. Jiang, *J. Am. Chem. Soc.,* 2009, **132**, 46-47.

Graphical Abstract

SnO$_2$/CNS composite composed of *in situ* generated ultrafine SnO$_2$ nanocrystals and graphitized carbon nanosheets (CNS) has been prepared through a crystal-facet-induced formation method. The obtained composite as the anode material for lithium-ion batteries exhibits superior electrochemical performance.